RSC Advances

PAPER

View Article Online
View Journal | View Issue

Cite this: *RSC Adv.*, 2020, **10**, 10980

Drug-loaded dual targeting graphene oxide-based molecularly imprinted composite and recognition of carcino-embryonic antigen

Shuang Han, *[a] Fu Teng,[a] Yuan Wang,[b] Liqiang Su,[a] Qiuxue Leng[a] and Haiyan Jiang[a]

Despite extensive research on functional graphene oxide for anticancer drug delivery, the sensitivity of traditional protein targeting ligands to the environment limits the practical applications of targeted drug delivery. A unique molecularly imprinted magnetic graphene oxide was used as a novel drug delivery system for the treatment of tumors. Molecularly imprinted polymers (MIPs) synthesized by molecular imprinting technology have the advantages of good stability against chemical and enzymatic attacks, high specificity for a target template, and resistance to harsh environments. In our work, the MIP was used for specificity to tumor cells with carcino-embryonic (CEA) tumor markers as the template, and dopamine as the functional monomer was grafted on boronic acid-functionalized magnetic graphene oxide. The structure of the nanoparticles was optimized and characterized in detail by vibrating sample magnetometry, X-ray diffraction analysis, UV-vis spectroscopy, and flow cytometry. The prepared polymer has magnetic properties, specific recognition to CEA, biocompatibility and pH sensitivity for drug delivery. Cell culture research was carried out on the tumor cells and normal cells. The composites exhibited dual targeting properties that not only magnetically target but also specifically increase the drug cytotoxicity to the tumor cells by selectively binding to CEA. On the basis of these results, this study developed a novel approach for targeting tumor cells for drug delivery without needing to modify the protein ligand.

Received 19th January 2020
Accepted 1st March 2020

DOI: 10.1039/d0ra00574f

rsc.li/rsc-advances

1. Introduction

Biomedical research on functional graphene oxide (GO) has been attracting a great deal of attention due to the special properties of GO that include large areas, low toxicity and multiple functional groups on the surface.[1,2] Therefore, GO may have promising applications in drug delivery.[3] For example, Xu's group reported a multifunctional theranostic nanoplatform based on graphene oxide (GO) and $MnWO_4$. GO, used as the carrier, possessed a high loading capacity for the anticancer drug doxorubicin hydrochloride (DOX) due to noncovalent forces and the drug release could be triggered by a lower pH value.[4] Jiang's group prepared a stimuli-responsive nanoplatform for the controllable delivery and release of drugs by integrating DNA aptamers with polydopamine graphene oxide nanosheets. The GO nanosheets acted as a nano-carrier for doxorubicin (DOX).[5] Li's group designed and synthesized heparin and polyethyleneimine–folic acid-modified graphene oxide to target biomaterials with a high loading capacity of DOX for enhanced cellular uptake.[6] Although many drug delivery systems with GO as the carrier have good performance to realize drug loading and release, their specificity to tumor cells is still a major concern and challenge.[7] The conventional drug loading system targets cells through the ligand of a specific receptor or antibody that is *in vivo* modified on the drug carrier. However, the sensitivity and weak stability of these protein targeting ligands greatly limits their applications. Therefore, an effective way to improve these issues is to develop an innovative antibody-free approach to treating tumors with drugs.

Molecular imprinting technology is a novel and rapidly developing technique used to synthesize polymers with selective recognition properties for a specific molecule.[8,9] Molecularly imprinted polymers (MIP), a product of the molecular imprinting technique, provide specific recognition sites for a designated substance, called the template, and can be the appropriate shape, dimension, and functional internal space to the template. Due to many advantages, such as a stable physicochemical nature that can resist chemical and enzymatic attack, specific recognition of the template molecule, low cost, and resistance to harsh environments, MIPs have excellent promise for practical application in the fields of separation,[10] detection,[11,12] and catalysis.[13] In addition, MIPs are considered as potential drug carrier candidates.[14] For example, Zaidi[15] reported that MIP-based DDS systems may be a real contender for drug delivery vehicle materials in biomedical devices. Luliński[16] reviewed imprinted

[a]College of Chemistry and Chemical Engineering, Qiqihar University, Qiqihar 161006, China. E-mail: iamhanshuang1982@163.com
[b]Heilongjiang Province Qiqihar Ecological Environment Monitoring Center, Qiqihar 161005, China

polymer-based drug delivery devices applied in modern pharmacotherapy and concluded that MIPs are promising materials in the construction of drug delivery devices because they can improve the delivery profiles or release over longer times and deliver drugs in a feedback regulated way, which is extremely important in modern pharmacotherapy. Tuwahatu[17] reported that MIPs possess properties that may complement the traditional delivery systems, such as a passive enhanced permeability and retention effect (EPR) in cancer tumors.

Tumor markers are a specific substance that exist on or are secreted from tumor cells. Carcino-embryonic antigen (CEA), a tumor marker, is a glycoprotein on the surface of several types of cancer tumor cells. Lai[18] prepared a MIP electrochemical sensor with CEA as the template, and dopamine (DA) as the imprinted monomer by controlling the electro-polymerization. This MIP sensor was demonstrated in testing CEA in a human serum sample with the detection limit as low as 0.2589 pg mL^{-1}. Yu[19] reported a molecular imprinting biosensor with CEA that was templated on a gold surface and a detection limit of 0.5 ng mL^{-1} was achieved. Wang[20] reported an electrochemical multiplexed immunoassay for the simultaneous determination of alpha-fetoprotein (AFP) and carcinoembryonic antigen (CEA) synthesized by the self-polymerization of dopamine (DA) on Fe_3O_4 nanoparticles, using AFP and CEA as the template proteins through molecular imprinting.

Here, our work tried to use CEA as a template combining molecular imprinting technology to prepare tumor marker-molecularly imprinted polymers to functionalize magnetic GO (MGO). The magnetically susceptible characteristics of MGO allow the composite to be potentially used for magnetically targeted drug delivery *via* an external localized magnetic field.[21] Some groups have reported magnetic imprinted materials dedicated to drug delivery. For example, Asadi[22] reported a new biodegradable cross-linker agent based on fructose for the fabrication of a brain-targeting MIP, where the magnetic structure of the prepared MIP facilitates the aggregation of carriers near the target tissue under a magnetic field. Hemmati[23] prepared a highly selective magnetic molecularly imprinted polymer (MMIP) as a drug delivery device synthesized by a sol–gel process composed of Tragacanth Gum (TG) cross-linker, Fe_3O_4/SiO_2 nanoparticles, and an *N*-vinyl imidazole (VI) functional monomer in the presence of the template, Quercetin (QC). Kazemi[24] reported magnetic letrozole imprinted polymer nanoparticles with the controlled release of the anticancer drug letrozole by precipitation polymerization using methacrylic acid (MAA) as the functional monomer in the presence of letrozole as the template and MAA-modified magnetite nanoparticles as the magnetic component. These magnetic MIPs were prepared with drugs as templates. This work reports the preparation of a drug delivery system with magnetic and molecularly imprinted targeting using CEA as a template. After the prepared composite reaches the intracorporal targeted position, imprinted cavities on the surface of the material recognize and capture CEA templates at the targeted position to give rise to specific binding to the tumor cells, which will achieve targeted drug delivery in a novel way. Thus, the dual targeting molecularly imprinted composite can be obtained with specific targeting and magnetic targeting. Not only will the dual targeting molecularly imprinted composite retain specific binding similar to the 'antigen–antibody', but also avoid the problem of a delivery system modified by an antibody.[25]

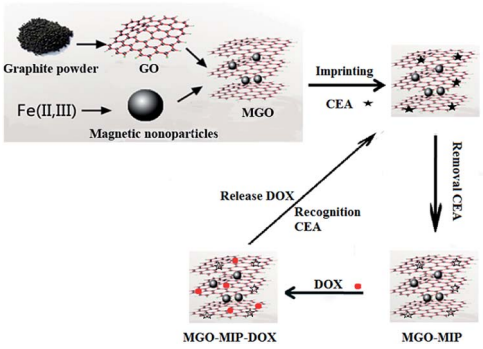

Fig. 1 Schematic of MGO-MIP-DOX preparation.

A schematic illustration of the preparation process is presented in Fig. 1. In this research, we designed a CEA-molecularly imprinted polymer using the molecular imprinting technique with the CEA tumor marker as a template, dopamine as the monomer, and boronic acid-functionalized MGO as the substrate for the dual targeting delivery of drugs to tumor cells. MGO as the substrate provides magnetism, a large surface for imprinted binding sites, drug efficient loading and pH sensitivity. After the polymerization and removal of CEA, the CEA-molecularly imprinted polymers (MGO-MIP) could recognize the tumor cells by the specific binding of CEA and thus eliminate the need for an antibody. Doxorubicin (DOX) is extensively used in the treatment of many tumors and is used as an example of an anticancer drug. The imprinted delivery system is employed to deliver the drug to the designated tumor cells by the specific targeting and magnetic targeting.

2. Experimental

2.1. Materials and reagents

HepG2 and L02 cells were obtained from Shanghai Honsun Biological Technology Co., Ltd (Shanghai, China). Graphite powder, ferric chloride ($FeCl_3 \cdot 6H_2O$), ethylene glycol, and $FeCl_2 \cdot 4H_2O$ were purchased from Shanghai Chemical Reagent Company (Shanghai, China). 4-Mercaptophenylboronic acid (MPB) were purchased from Sigma-Aldrich Co. (St. Louis, MO). Doxorubicin (DOX), dopamine (DA), and dimethyl sulfoxide (DMSO) were purchased from Shanghai Aladdin Bio-Chem Technology Corporation (Shanghai, China). Carcino-embryonic antigen (CEA), immunoglobulin (IgG), cancer antigen 125 (CA125), and glucose (Glu) were purchased from Shanghai Linc-Bio Science Co. LTD (Shanghai, China).

2.2. Preparation of MGO-MIP

Graphene oxide was prepared through a previously reported approach.[26] The MGO nanocomposite was synthesized using the chemical co-precipitation method similar to that reported previously as follows.[27] GO (200 mg) was sonicated into 45 mL of

NaOH aqueous solution (pH 12) for 180 min to transform the carboxylic acid groups to carboxylate anions, followed by thorough dialysis until the dialysate became neutral. After that, the product was condensed to 10 mL and the solution of $FeCl_3 \cdot 6H_2O$ (150 mg) and $FeCl_2 \cdot 4H_2O$ (400 mg) in water (20 mL) was added to the product. The mixture was stirred at 80 °C for 20 min. Subsequently, 2 mL of ammonium hydroxide (NH_4OH) was added, and stirred at 80 °C for another 3 h. After that, the mixture was washed with water to a neutral pH and dried. Boronic acid-functionalized MGO were also prepared. 10 mg of MGO were dispersed into 10 mL of methanol including 30 mg of 4-mercaptophenylboronic acid, and then the mixture was sonicated for 6 h. After that, the product was recovered magnetically and then washed using methanol to remove excess 4-mercaptophenylboronic acid.

The MGO-MIP composite was prepared as follows. First, 1.0 g of boronic acid-functionalized MGO was added into 25 mL of 450 mM phosphate buffer (pH 8.5). After that, a certain amount of CEA and 15 mg of DA were added to the above mixture and sonicated for 25 min. Next, 20 mg of ammonium persulfate was mixed into the mixture to initiate polymerization for 60 min. Finally, the prepared product was washed using ethanol as the solvent to remove the CEA template. The corresponding non-imprinted polymer (MGO-NIP) was synthesized with the same method as MGO-MIP, except without CEA.

2.3. DOX loading

20 mL of water was added to DOX (20 mg) and MGO-MIP (20 mg) and stirred. After that, the polymers were magnetically separated then washed several times until the supernatant became colorless. Lastly, the collected MGO-MIP-DOX particles were freeze-dried for research.

For comparison, MGO-NIP-DOX was also prepared with the same method as the above MGO-MIP-DOX except for with the addition of CEA.

2.4. Apparatus

The X-ray diffraction (XRD) patterns were recorded on a German Bruker D8-FOCUS X-ray Diffraction (100 mm × 2.1 mm, 1.7 μm). Magnetic properties were recorded using a LakeShore 7307 (Lakeshore Cryotronic) vibration sample magnetometer (VSM) at 300 K. Flow cytometry was carried out on a flow cytometer (BD, C6). UPLC analysis was performed on the Waters ACQUITY UPLC system containing an ACQUITY UPLC-BEH column (100 mm × 2.1 mm, 1.7 μm).

2.5. Adsorption and recognition evaluation

10 mg of MGO-MIP or MGO-NIP composite was added to 10 mL of CEA solution, respectively. When achieving adsorption, particles were collected and the mass of CEA binding to particles could be calculated through the difference of the concentration value before and after the adsorption to polymers using UPLC analysis. The mobile phase consisted of 80% acetonitrile and 20% de-ionized water, with the flow rate of 0.5 mL min^{-1}. The injection volume was 20 μL and detected at 294 nm. The adsorption capacity (Q) can be measured following the equation:

$$Q = (C_1 - C_2)V/W \quad (1)$$

C_1 and C_2 is the CEA concentration before and after binding. V is the volume of the solution and W is the mass of the MGO-MIP or MGO-NIP.

2.6. Selectivity binding experiments

To verify the specificity of MGO-MIP-DOX for CEA, 10 mg of different hybrids were mixed into 10 mL of 5 nmol L^{-1} CEA, CA125, Glu and lgG solutions, respectively. This procedure was the same as the previous adsorption and recognition evaluation.

2.7. Drug desorption studies

In the drug desorption experiments, 25 mg of MGO-MIP-DOX was added into 25 mL of buffers at a series of pH values and stirred at 37 °C. The particles were magnetically moved. The concentrations of DOX were determined by UPLC with the absorbance detected at 254 nm under the UPLC mobile phase (methanol : HAc : water = 80 : 0.3 : 19.7) at a flow rate of 0.5 mL min^{-1}.

2.8. Cell viability

An MTT assay was used to investigate the lethality of MGO-MIP-DOX to tumor cells.[28] HepG2 and L02 cells were seeded in culture medium (80 μL) on 96-well plates at a density of 1×10^4 cells per well incubated at 37 °C for 20 h, respectively. After that the medium was removed and 80 μL of a different culture medium including a particular agent (MGO-MIP or MGO-MIP-DOX) was added for another 20 h. Subsequently, the culture medium was replaced by fresh medium containing 3-(4,5-dimethylthiazol-2-yl)-2,5-diphenyltetrazolium bromide (MTT) (final concentration of 0.5 mg mL^{-1}). The cells were incubated for another 3 h. Then, the supernatant was replaced with dimethyl sulfoxide (DMSO) (80 μL) and plates were shaken for 10 min. The absorbance of the solution was obtained through a microplate reader at a wavelength of 570 nm to measure the optical density (OD) value. The cell viability was calculated from the following equation.[29]

$$\text{Cell viability} = \text{ODtreated/ODcontrol} \times 100\% \quad (2)$$

where ODtreated was determined from the cells treated by a particular agent and ODcontrol was determined from the cells without any treatments.

2.9. Flow cytometric analysis

Flow cytometry was applied to measure the cell apoptosis of MGO-MIP-DOX by recording the cell fluorescence. After that, 30 μg mL^{-1} of different particles in the presence of 30 μL DMSO was mixed into the HepG2 cells and incubated at 37 °C for 6 h.

2.10. Degradation tests

10 mg of MGO-MIP-DOX was mixed with 10 mL of buffer solution, which was pH 4.5, over different times at 37 °C, respectively. After that, particles were collected magnetically, dried and weighed.

3. Results and discussion

3.1. Effects of imprinted conditions

The content of MGO in MGO-MIP may influence the number of imprinted cavities, thus directly affecting the ability of MGO-MIP-DOX to specifically recognize tumor cells. At the same time, the content of MGO determines the magnetic properties of MGO-MIP. In this study, the influence of MGO content on the binding capacity of MGO-MIP for CEA and the magnetic saturation of MGO-MIP was studied by keeping the other conditions the same. As can be seen in Fig. 2, the adsorption capacity reached the maximum when the dosage of MGO was 20 g L^{-1}. This could be because having less of the MGO carrier resulted in binding sites that were partially embedded deeply into the polymers, which blocked the template in the imprinted sites. However, a larger amount of the MGO carrier resulted in fewer binding sites per unit surface of the MGO carrier. The maximum saturation magnetization of MGO-MIP increased with increasing MGO carrier content. These results were consistent with the previously reported finding[30] that the percentage of magnetic core in the range of 20–25% provide the most effective magnetic imprinted materials. Finally, 20 g L^{-1} MGO carrier was chosen as the optimal amount.

In this research, dopamine (DA) was used as the functional monomer and it was anticipated that the hydroxyl and amide functional groups of DA would form non-covalent interactions with CEA. During the polymerization, template CEA was trapped in the polymer matrix since it could interact with the dopamine units. Hydrogen bonding could occur between the template and the dopamine units. Next, the content of DA was kept constant and the amount of CEA was gradually increased to measure the adsorption capacity of each synthesized polymer. As shown in Fig. 3. The concentration of CEA in the molecular imprinting polymerization was optimized. The MGO-MIP first displayed an increased binding with CEA in the concentration range of 10 mg L^{-1} to 40 mg L^{-1}, then reduced as it exceeded 40 mg L^{-1}. The phenomenon may be attributed to the interaction force between the template and functional monomer that directly influences the recognition of MGO-MIP. When the content of CEA was too large or too little, the interaction force between the template and functional monomer was weak and the functional groups in the prepared MGO-MIP were distributed randomly. Consequently, the cavities formed in the MGO-MIP do not match with the template molecules, which will lower the recognition performance of MGO-MIP. In contrast, with an ideal ratio, the interaction force between the template molecule and the functional monomer is strong, so there will be more selectivity recognition sites and cavities matching the template molecules in MGO-MIP. Consequently, the CEA concentration in the synthesis procedure was adopted to be 40 mg L^{-1}.

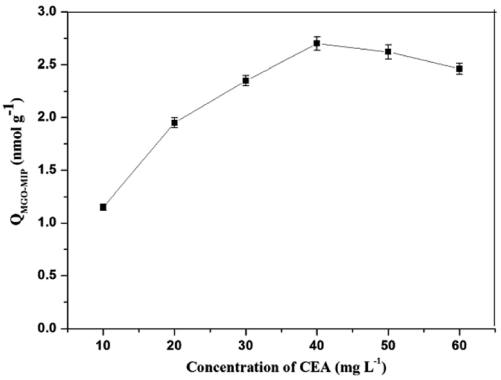

Fig. 3 Effect of concentration of template CEA.

3.2. Characterization of MGO-MIP-DOX

Fig. 4 exhibits the XRD patterns of GO, MGO and MGO-MIP. As seen in Fig. 4a, the diffraction peak at $2\theta = 11°$ is ascribed to the (002) crystal of GO. In Fig. 4b, the peak positions at corresponding 2θ value are indexed as the (220), (311), (400), (422), (511) and (440) planes, suggesting that a spinel structure Fe_3O_4 has been prepared.[31,32] In Fig. 4c, the characteristic peaks of GO

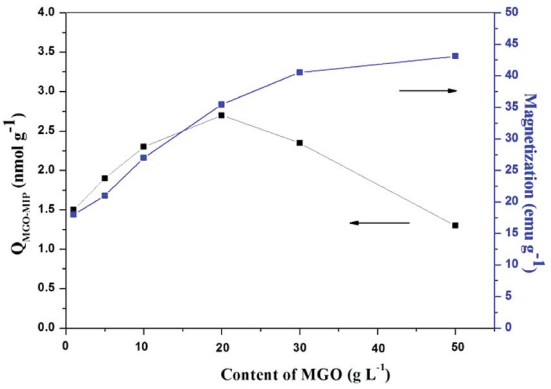

Fig. 2 The effects of different dosages of MGO on the adsorption capacity and magnetic properties of MGO-MIP.

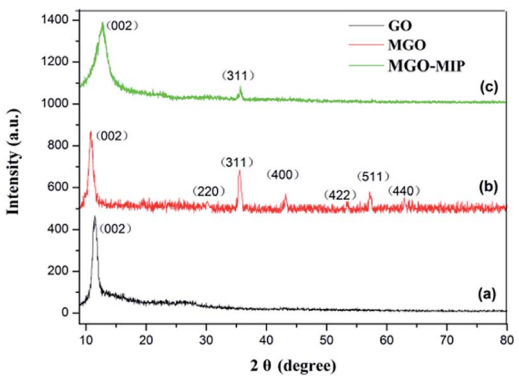

Fig. 4 XRD patterns of GO (a), MGO (b), and MGO-MIP (c).

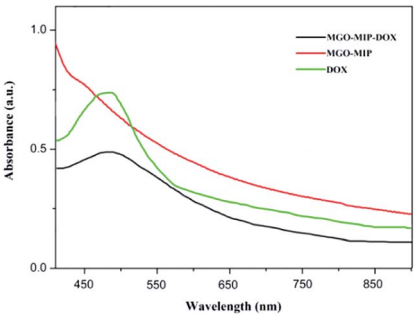

Fig. 5 UV-vis spectra of GO, MGO-MIP and MGO-MIP-DOX.

and Fe_3O_4 are present and peak positions are the same, which verifies that the crystal structure of each is not substantially changed. These results further suggest the successful preparation of a MGO-MIP composite.

Fig. 5 shows the ultraviolet-visible absorption spectra of DOX, MGO-MIP and MGO-MIP-DOX composites. The evidence of drug loading on MGO-MIP is presented. The absorption feature of DOX was at 490 nm and the absorption peak was slightly red-shifted after the noncovalent loading of DOX on MGO-MIP, verifying the interactions between DOX and MGO-MIP.[33]

From the BET analysis, the surface area of MGO-MIP and MGO-NIP was measured to be 584.152 $m^2\ g^{-1}$ and 274.254 $m^2\ g^{-1}$, respectively (Table 1). With regard to MGO-MIP, the surface area obviously increases following the washing of CEA in the molecular imprinting procedure, which results in more pore structures. Moreover, the unique structures of MGO-MIP with a large surface area and pore size are fit for the binding of target CEA.

The morphology of MGO-MIP and MGO-NIP was assessed by SEM analysis (Fig. 6). The surface of MGO-NIP was smoother than that of MGO-MIP. The presence of more pores or cavities on MGO-MIP suggests that the porosity generated on the surface of MGO-MIP is due to the template extraction and the results were consistent with the BET analysis.

The magnetic properties of MGO, MGO-MIP and MGO-MIP-DOX were probed using VSM (Fig. 7). The saturation magnetization (M_s) value of MGO-MIP-DOX was lower compared to the M_s value of MGO and MGO-MIP, due to the contributions of DOX and the imprinted polymer film, which induced the presence of magnetite. The M_s value of MGO-MIP-DOX was 29.85 emu g^{-1}, confirming the desirable magnetic behavior of MGO-MIP-DOX for application in magnetically guidable drug delivery.

Table 1 Surface properties of MGO-MIP and MGO-NIP

Polymer	BET surface area ($m^2\ g^{-1}$)	Pore volume ($cm^2\ g^{-1}$)	Pore size (nm)
MGO-MIP	584.152	0.541	15.692
MGO-NIP	274.254	0.214	19.956

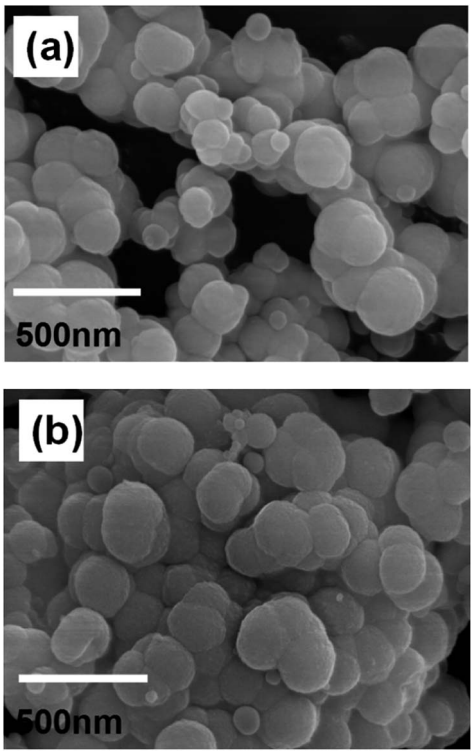

Fig. 6 The morphology of MGO-NIP (a) and MGO-MIP (b).

3.3. Adsorption isotherms modeling

The binding properties of MGO-MIP and MGO-NIP to CEA were studied by the static equilibrium adsorption and then the equilibrium data were fitted to the Langmuir and Freundlich isotherm models. From the fitting of the experimental data to two isotherm models, the adsorption equilibrium constants and linear regression values are listed in Table 2. In Fig. 8, two models for adsorption using non-linear regression are shown. The CEA adsorbed on MGO-MIP was greater than that of MGO-NIP, indicating that the CEA preferentially adsorbs to MGO-MIP. Fitting the experimental data with the two isotherm equations, the Langmuir isotherm model fit the equilibrium data much better than the Freundlich model, indicating that the polymers exhibit monolayer molecular adsorption.

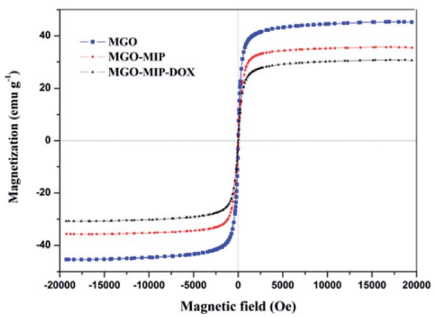

Fig. 7 Magnetization curves of MGO, MGO-MIP and MGO-MIP-DOX.

Table 2 Adsorption isotherm constants for CEA adsorption onto MGO-MIP and MGO-NIP

	Langmuir equation			Freundlich equation		
Polymers	Q_m (nmol g^{-1})	K_L (L nmol^{-1})	R^2	K_F (nmol g^{-1})	$1/n$	R^2
MGO-MIP	2.61	81.83	0.9993	0.490	0.2731	0.7930
MGO-NIP	0.52	16.1	0.9988	0.055	0.3485	0.8895

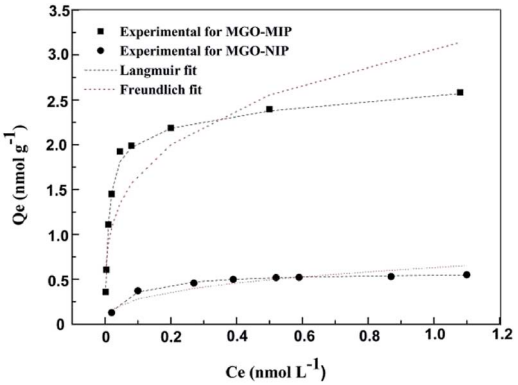

Fig. 8 The adsorption isotherms of CEA onto MGO-MIP and MGO-NIP.

3.4. Specific recognition of MGO-MIP-DOX

The selective binding of MGO-MIP-DOX for tumor marker CEA is significant for targeting tumor cells in biological samples that include several possible interference species. The selectivity of MGO-MIP-DOX for CEA was further demonstrated using Glu, lgG and CA125 (cancer marker) as interferences. As shown in Fig. 9, the MGO-MIP and MGO-MIP-DOX imprinted polymers exhibited relatively higher binding affinities for CEA than that of the non-template interference. This phenomenon can be ascribed to how the imprinted polymers can bind to the template CEA because of the presence of imprinted cavities.

Moreover, it has been shown that MGO-NIP-DOX exhibited weak adsorption to all the substances, suggesting that MGO-NIP-DOX had no ability to specifically bind to CEA. Although MGO-MIP-DOX showed a relatively lower adsorption capacity than MGO-MIP owing to the DOX loading, MGO-MIP-DOX exhibited an appreciable adsorption capacity to CEA. In addition, the imprinting factor is generally defined as a vital indicator that evaluates the specificity of molecularly imprinted polymers. In this research, the imprinting factor can be determined as the ratio of the adsorption capacity of MGO-MIP-DOX for CEA to that of MGO-NIP-DOX. Thus, the imprinting factor was 5.93, suggesting the specific binding of MGO-MIP-DOX for CEA. Furthermore, it can be implied that the prepared MGO-MIP-DOX can be applied for the effective specific recognition of tumor cells without the influence of other interference substance.

3.5. Drug desorption tests *in vitro*

The drug desorption properties of MGO-MIP-DOX and MGO-NIP-DOX were further researched and the drug desorption curves at different pH values are shown in Fig. 10. The amount of DOX released from MGO-MIP-DOX after 10 h at pH 7.0 was only 3.5%. Nevertheless, 40% and 22% release percentages could be accomplished within 10 h at pH 5.0 and pH 6.0 buffer solutions, respectively. The process of template removal did not have a significant influence on the drug desorption upon comparing the desorption of MGO-MIP-DOX and MGO-NIP-DOX. The properties of the pH-responsive drug desorption were ascribed to a stronger non-specific adsorption between the polymers and DOX that possess numerous –OH groups under more neutral conditions than under acidic conditions. Moreover, supramolecular π–π stacking between the carbonaceous framework of GO and aromatic DOX molecules may be interfered with and broken in a mild acidic environment.[34] The pH-

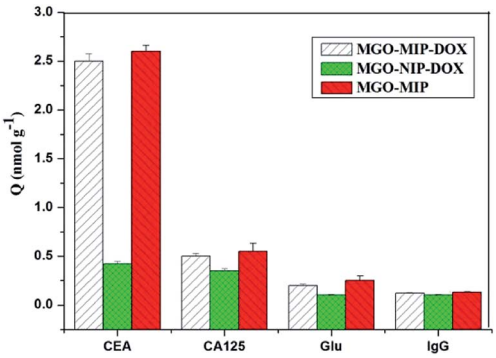

Fig. 9 Absorption capacity of MGO-MIP-DOX, MGO-NIP-DOX and MGO-MIP for different targets.

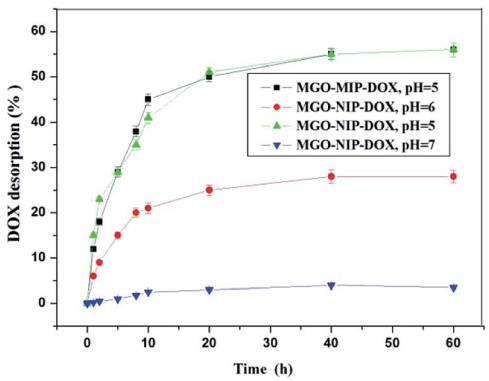

Fig. 10 The desorption of DOX from MGO-MIP-DOX and MGO-NIP-DOX at different pH values.

Table 3 Model analysis of the release mechanism

Kinetic models equation (M_t/M_∞)	Zero order, K_0t	First order, $1 - \exp(-K_1t)$	Higuchi $K_Ht^{1/2}$
MGO-MIP-DOX, pH = 5	$R^2 = 0.6585$	$R^2 = 0.7514$	$R^2 = 0.9102$, $K_H = 7.3889$
MGO-NIP-DOX, pH = 5	$R^2 = 0.7223$	$R^2 = 0.8283$	$R^2 = 0.9349$, $K_H = 7.3185$
MGO-MIP-DOX, pH = 6	$R^2 = 0.6711$	$R^2 = 0.7099$	$R^2 = 0.9115$, $K_H = 3.7680$
MGO-MIP-DOX, pH = 7	$R^2 = 0.7151$	$R^2 = 0.7174$	$R^2 = 0.9137$, $K_H = 0.5418$

sensitive desorption behavior that is consistent with previous research can help to deliver antitumor drugs.[35] As is well-known, in normal tissues the pH value is about 7.4, while it becomes lower in the tumor position and even lower (4.5–6.0) in endosomes and lysosomes.

To investigate the mechanism of drug desorption from the polymers, the experimental data were fitted to zero-order, first-order and Higuchi models. Table 3 shows the calculated values of release constants together with the regression coefficients (R^2) on the basis of regression analysis. It may be concluded that the Higuchi model fit best with the experimental data, which may suggest that the dominant release mechanism is probably controlled by diffusion.

3.6. Cytotoxicity studies against cancer cells and flow cytometry analysis

Viability experiments were conducted on two different kinds of cells to research the specific lethality effect of the MGO-MIP-DOX composite to target HepG2 tumor cells. Fig. 11 presents the relative viability of two kinds of cells cultured with several particles, respectively. After 24 h, 50 μg mL^{-1} of MGO-MIP composite as the carrier did not present significant cytotoxicity to HepG2 tumor cells and L02 normal cells, suggesting good the biocompatibility of MGO-MIP under these conditions. These results were consistent with a published report that no detectable MIP toxicity was found in either cell systems or mouse models. MGO-MIP-DOX presented a greater lethality to target HepG2 tumor cells than MGO-MIP, confirming that the cytotoxicity to cells was the result of drug loading. MGO-MIP-DOX showed a greater lethality to target tumor cells than L02 normal cells at any concentration. That might be ascribed to the presence of more CEA on the surface of the HepG2 tumor cells, which could bind to MGO-MIP-DOX and increase the cytotoxicity to the cells. MGO-MIP-DOX showed a significant lethality to HepG2 tumor cells owing to the specific CEA imprinted recognition sites of MGO-MIP-DOX, which increased the cellular uptake of the loading drug. Moreover, MGO-MIP-DOX did not destroy the normal cells, verifying the safety of chemotherapy.

It is clear in Fig. 12 that the percentages of apoptosis induced by MGO-NIP-DOX and MGO-MIP-DOX were 28.3% and 96.7% after 6 h of treatment, respectively. This result further suggested that the enhanced cell apoptosis related to the specific recognition properties of the imprinted polymers to tumor cells. Moreover, the percentage of apoptosis induced by MGO-MIP was only 6.4%, revealing its excellent biocompatibility. The results further verified the conclusions drawn from the MTT assay.

3.7. Degradation study

The remaining mass of MGO-MIP-DOX is shown at different times through its degradation (Fig. 13). The mass remaining was about 85% after 70 h and the degradation may have begun from the dopamine in the polymers.

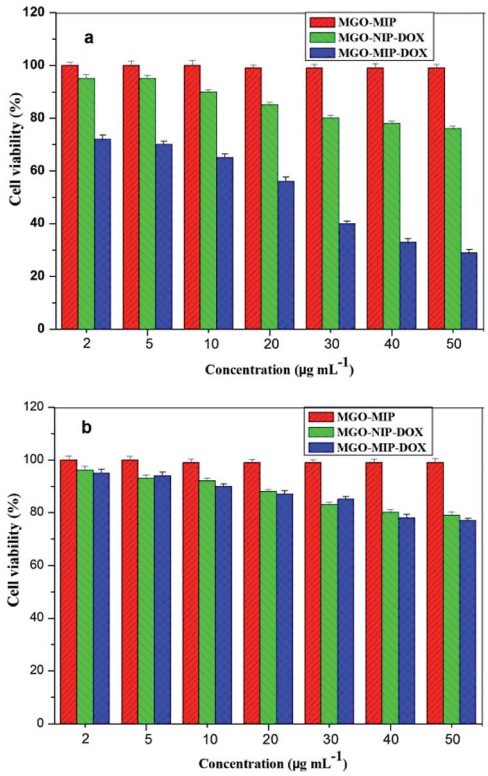

Fig. 11 Cell viability of HepG2 cells (a) and L02 cells (b) after being treated by MGO-MIP-DOX, MGO-NIP-DOX and MGO-MIP nanoparticles.

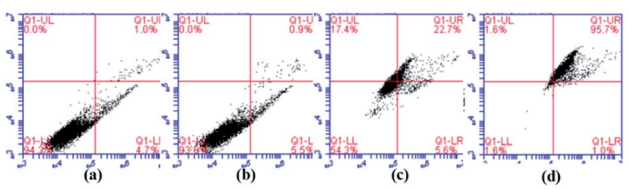

Fig. 12 Flow cytometric analysis of HepG2 cells without any treatment (a), HepG2 cells incubated with 30 μg mL^{-1} of MGO-MIP (b), MGO-NIP-DOX (c), and MGO-MIP-DOX (d) for 6 h.

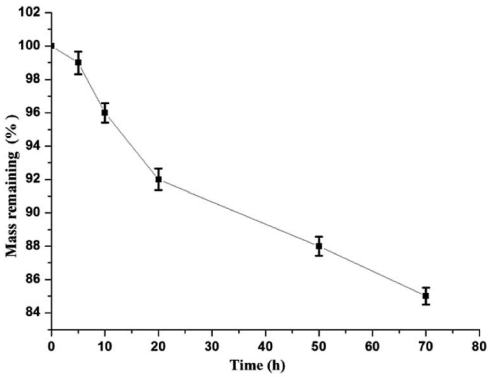

Fig. 13 The mass remaining of MGO-MIP-DOX through degradation *in vitro*.

4. Conclusion

In summary, we have developed a molecularly imprinted polymer based on MGO with CEA as the template for the specific delivery of DOX. This novel hybrid combines the unique advantages of MIPs that show a high selectivity recognition for CEA without interference. Due to the larger saturation magnetization of MGO-MIP-DOX, the hybrid shows an efficient way to magnetically target. Furthermore, MGO-MIP-DOX presented a significant suppression of cell viability to target tumor cells rather than normal cells. MGO-MIP-DOX has specificity, excellent biocompatibility and pH-responsive release. Thus, it is believed that the MGO-MIP-DOX hybrid could be used as an advanced drug delivery system to improve the specificity and to overcome the drawback of traditional modifying ligands.

Funding

This study was funded by Heilongjiang Province Science Foundation for Youths (No: QC2018073), the Fundamental Research Funds in Heilongjiang Provincial Universities (No: 135409210), and Social Development Public Relations Project of Qiqihar Science and Technology Bureau (No: SFZD-2019151).

Conflicts of interest

The authors declare that they have no conflict of interest.

References

1 R. Tao, C. Wang, C. Zhang, *et al.*, Characterization, cytotoxicity and genotoxicity of graphene oxide and folate coupled chitosan nanocomposites loading polyprenol and fullerene based nanoemulsion against MHCC97H cells, *J. Biomed. Nanotechnol.*, 2019, **15**(3), 555–570.

2 S. Zheng, Z. Jin, C. Han, *et al.*, Graphene quantum dots-decorated hollow copper sulfide nanoparticles for controlled intracellular drug release and enhanced photothermal-chemotherapy, *J. Mater. Sci.*, 2020, **55**(3), 1184–1197.

3 Y. Liu, J. Peng, S. Wang, *et al.*, Molybdenum disulfide/graphene oxide nanocomposites show favorable lung targeting and enhanced drug loading/tumor-killing efficacy with improved biocompatibility, *NPG Asia Mater.*, 2018, **10**(1), e458.

4 X. Chang, Y. Zhang, P. Xu, *et al.*, Graphene oxide/MnWO4 nanocomposite for magnetic resonance/photoacoustic dual-model imaging and tumor photothermo-chemotherapy, *Carbon*, 2018, **138**, 397–409.

5 W. Jiang, F. Mo, Y. Lin, *et al.*, Tumor targeting dual stimuli responsive controllable release nanoplatform based on DNA-conjugated reduced graphene oxide for chemo-photothermal synergetic cancer therapy, *J. Mater. Chem. B*, 2018, **6**(26), 4360–4367.

6 J. Li, X. Liang, J. Zhang, *et al.*, Inhibiting pulmonary metastasis of breast cancer based on dual-targeting graphene oxide with high stability and drug loading capacity, *Nanomedicine*, 2018, **14**(4), 1237–1248.

7 A. C. Anselmo and S. Mitragotri, Impact of particle elasticity on particle-based drug delivery systems, *Adv. Drug Delivery Rev.*, 2017, **108**, 51–67.

8 S. M. E. Nilsson, S. Suriyanarayanan, S. Kathiravan, *et al.*, Enantioselective hyperporous molecularly imprinted thin film polymers, *RSC Adv.*, 2019, **9**(58), 33653–33656.

9 W. Huang, X. Hou, Y. Tong, *et al.*, Determination of sialic acid in serum samples by dispersive solid-phase extraction based on boronate-affinity magnetic hollow molecularly imprinted polymer sorbent, *RSC Adv.*, 2019, **9**(10), 5394–5401.

10 M. Rutkowska, J. Płotka-Wasylka, C. Morrison, *et al.*, Application of molecularly imprinted polymers in analytical chiral separations and analysis, *TrAC, Trends Anal. Chem.*, 2018, **102**, 91–102.

11 T. Zhou, L. Ding, G. Che, *et al.*, Recent advances and trends of molecularly imprinted polymers for specific recognition in aqueous matrix: preparation and application in sample pretreatment, *TrAC, Trends Anal. Chem.*, 2019, **114**, 11–28.

12 O. I. Parisi, C. Morelli, F. Puoci, *et al.*, Magnetic molecularly imprinted polymers (MMIPs) for carbazole derivative release in targeted cancer therapy, *J. Mater. Chem. B*, 2014, **2**(38), 6619–6625.

13 M. Sobiech, P. Bujak, P. Luliński, *et al.*, Semiconductor nanocrystal–polymer hybrid nanomaterials and their application in molecular imprinting, *Nanoscale*, 2019, **11**(25), 12030–12074.

14 S. Han, L. Su, M. Zhai, *et al.*, A molecularly imprinted composite based on graphene oxide for targeted drug delivery to tumor cells, *J. Mater. Sci.*, 2019, **54**(4), 3331–3341.

15 S. A. Zaidi, Latest trends in molecular imprinted polymer based drug delivery systems, *RSC Adv.*, 2016, **6**(91), 88807–88819.

16 P. Luliński, Molecularly imprinted polymers based drug delivery devices: a way to application in modern pharmacotherapy. A review, *Mater. Sci. Eng., C*, 2017, **76**, 1344–1353.

17 C. A. Tuwahatu, C. C. Yeung, Y. W. Lam, *et al.*, The molecularly imprinted polymer essentials: curation of

anticancer, ophthalmic, and projected gene therapy drug delivery systems, *J. Controlled Release*, 2018, **287**, 24–34.

18 Y. Lai, Y. Deng, G. Yang, *et al.*, Molecular imprinting polymers electrochemical sensor based on AuNPs/PTh modified GCE for highly sensitive detection of carcinomaembryonic antigen, *J. Biomed. Nanotechnol.*, 2018, **14**(10), 1688–1694.

19 Y. Yu, Q. Zhang, J. Buscaglia, *et al.*, Quantitative real-time detection of carcinoembryonic antigen (CEA) from pancreatic cyst fluid using 3-D surface molecular imprinting, *Analyst*, 2016, **141**(14), 4424–4431.

20 D. Wang, N. Gan, H. Zhang, *et al.*, Simultaneous electrochemical immunoassay using graphene–Au grafted recombinant apoferritin-encoded metallic labels as signal tags and dual-template magnetic molecular imprinted polymer as capture probes, *Biosens. Bioelectron.*, 2015, **65**, 78–82.

21 A. K. Swain, L. Pradhan and D. Bahadur, Polymer stabilized Fe_3O_4-graphene as an amphiphilic drug carrier for thermo-chemotherapy of cancer, *ACS Appl. Mater. Interfaces*, 2015, **7**(15), 8013–8022.

22 E. Asadi, M. Abdouss, R. M. Leblanc, *et al.*, Synthesis, characterization and in vivo drug delivery study of a biodegradable nano-structured molecularly imprinted polymer based on cross-linker of fructose, *Polymer*, 2016, **97**, 226–237.

23 K. Hemmati, A. Masoumi and M. Ghaemy, Tragacanth gum-based nanogel as a superparamagnetic molecularly imprinted polymer for quercetin recognition and controlled release, *Carbohydr. Polym.*, 2016, **136**, 630–640.

24 S. Kazemi, A. A. Sarabi and M. Abdouss, Synthesis and characterization of magnetic molecularly imprinted polymer nanoparticles for controlled release of letrozole, *Korean J. Chem. Eng.*, 2016, **33**(11), 3289–3297.

25 J. Zhou, N. Gan and T. H. Li, Ultratrace detection of c-reactive protein by a piezoelectric immunosensor based on Fe_3O_4@SiO_2 magnetic capture nanoprobes and hrp-antibody co-immobilized nano gold as signal tags, *Sens. Actuators, B*, 2013, **178**, 494–500.

26 Y. Zhu, S. Murali, W. Cai, *et al.*, Graphene and graphene oxide: synthesis, properties, and applications, *Adv. Mater.*, 2010, **22**(35), 3906–3924.

27 L. Z. Bai, D. L. Zhao, Y. Xu, *et al.*, Inductive heating property of graphene oxide-Fe_3O_4 nanoparticles hybrid in an AC magnetic field for localized hyperthermia, *Mater. Lett.*, 2012, **68**, 399–401.

28 E. Song, W. Han, C. Li, *et al.*, Hyaluronic acid-decorated graphene oxide nanohybrids as nanocarriers for targeted and pH-responsive anticancer drug delivery, *ACS Appl. Mater. Interfaces*, 2014, **6**(15), 11882–11890.

29 P. Liang, D. Zhao, C. Q. Wang, *et al.*, Facile preparation of heparin/$CaCO_3$/CaP hybrid nano-carriers with controllable size for anticancer drug delivery, *Colloids Surf., B*, 2013, **102**, 783–788.

30 M. Villar-Navarro, M. J. Martín-Valero, R. M. Fernández-Torres, *et al.*, Easy, fast and environmental friendly method for the simultaneous extraction of the 16 EPA PAHs using magnetic molecular imprinted polymers (mag-MIPs), *J. Chromatogr. B: Anal. Technol. Biomed. Life Sci.*, 2017, **1044**, 63–69.

31 S. Han, X. Li, Y. Wang, *et al.*, Multifunctional imprinted polymers based on CdTe/CdS and magnetic graphene oxide for selective recognition and separation of pt-octylphenol, *Chem. Eng. J.*, 2015, **271**, 87–95.

32 J. Kurczewska, M. Cegłowski, P. Pecyna, *et al.*, Molecularly imprinted polymer as drug delivery carrier in alginate dressing, *Mater. Lett.*, 2017, **201**, 46–49.

33 M. L. Chen, Y. J. He, X. W. Chen, *et al.*, Quantum-dot-conjugated graphene as a probe for simultaneous cancer-targeted fluorescent imaging, tracking, and monitoring drug delivery, *Bioconjugate Chem.*, 2013, **24**(3), 387–397.

34 S. Mohapatra, S. R. Rout, R. K. Das, *et al.*, Highly hydrophilic luminescent magnetic mesoporous carbon nanospheres for controlled release of anticancer drug and multimodal imaging, *Langmuir*, 2016, **32**(6), 1611–1620.

35 M. Q. Gong, J. L. Wu, B. Chen, *et al.*, Self-assembled polymer/inorganic hybrid nanovesicles for multiple drug delivery to overcome drug resistance in cancer chemotherapy, *Langmuir*, 2015, **31**(18), 5115–5122.

